JOURNAL OF COMPUTATIONAL PHYSICS **138,** 858–880 (1997)
ARTICLE NO. CP975663

Hybrid Spectral Element/Asymptotic Method for Boundary Layers Problems

U. Zrahia*, S. A. Orszag,* and M. Israeli†

**Fluid Dynamics Research Center, Princeton University Princeton, New Jersey 08544-0710;*
†Computer Science Department, Technion, Israel Institute of Technology, Haifa 32000, Israel

Received September 5, 1996

An efficient high-order approach to multi-dimensional problems with boundary or interior layers is presented. It combines a coarse grid penalty-spectral element method with a local one-dimensional asymptotic approximation. The solution so obtained is improved by numerical manipulations on the same coarse grid. Examples of interior and boundary layer problems are presented.

1. INTRODUCTION

Singular perturbation problems arise frequently in solid mechanic, flow and heat transfer, and semiconductor device simulation [1–3]. They usually occur when the coefficient of the highest-order derivative in the governing differential equation, ε, satisfies $\varepsilon \ll 1$. In this case the solutions exhibit narrow boundary layers of a characteristic width depending on ε. Solutions for this type of problem can be obtained by numerical methods, asymptotic techniques [4], or hybrid methods [5] which are based on a combination of numerical and asymptotic solutions. Singular perturbation problems become increasingly more difficult to solve numerically as ε becomes smaller. Indeed, if a uniform grid is used, a large number of grid points would be required to resolve the boundary layers or, an adaptive nonuniform mesh could be used [6, 7, 4]. However, it remains a challenge to obtain accurate results efficiently.

Asymptotic methods are useful if it is possible to obtain an approximate solution in terms of the small parameter ε. For such singular perturbation problems, the asymptotic solution is usually composed of an inner solution, which is valid in the neighborhood of the boundary layer and an outer solution which is valid away from the boundary layer. The order of accuracy of the asymptotic approximation is

0021-9991/97 $25.00

$O(\varepsilon^{j+1})$, where j is the order of the asymptotic expansion. Flaherty and O'Malley [10] developed an algorithm which solves numerically for the inner and outer asymptotic solutions using a standard numerical method. A representative hybrid technique is the "booster method" [5] which combines an asymptotic solution of accuracy $O(\varepsilon^{j+1})$ [10] with standard discretization methods. By this method, the numerical error is reduced by a factor $O(\varepsilon^{j+1})$. The booster approach could be difficult to implement for multidimensional problems in complex geometries, when an asymptotic solution cannot be easily obtained. A more accurate procedure, albeit a much more expensive one, is to replace the asymptotic inner or outer solutions by multidimensional numerical solutions [12].

In this work we present an alternative way to efficiently obtain asymptotic solutions for multidimensional boundary and interior layer problems. An approximate solution, u_A, which is a composite of an inner solution, u_{i}, and an outer solution, u_{o}, is calculated. The outer solution which is valid away from the boundary layer is not an asymptotic solution of the reduced problem but a solution to a modified problem. It is calculated numerically on a coarse mesh (see Section 3). The inner solution, u_{i}, is valid in and in the neighborhood of the boundary layer (see Section 4). The solution for u_A is of a low computational cost because its outer component is calculated numerically on a coarse grid in the domain of the problem while its inner component involves only one-dimensional analytical computations. This composite solution is used as a first approximation and is improved by solving a modified equation numerically on the same coarse grid as for the outer solution (see Section 5).

2. OVERVIEW OF THE METHOD

Let us consider a boundary value problem for the partial differential equation:

$$\varepsilon\nabla^2 u + \mathbf{V}\cdot\nabla u + au = f \quad \text{for } \mathbf{x}\in\Omega, \tag{1}$$

where $u, f, \mathbf{V}$, are functions of $\mathbf{x}\in\Omega\subset\mathscr{R}^d$ and d is the number of space dimensions. We assume that: ε is a small positive parameter, a is a negative constant; $f(\mathbf{x})$ may have a finite number of jump discontinuities while u is once differentiable in Ω and piecewise twice differentiable.

Let Γ_b be the part of the boundary, $\Gamma\equiv\partial\Omega$, which supports a boundary layer, and let Γ_g be the complement of Γ_b in Γ. We assume that

$$u = U_g \quad \text{on } \Gamma_g \tag{2}$$

and

$$u = U_b \quad \text{on } \Gamma_b \tag{3}$$

and lead to a unique solution of the problem.

The solution of (1)–(3) may exhibit two types of layers: interior or boundary layers. Boundary layers are located at boundaries of the domain (i.e., Γ_b). Their

thickness and location depend on the angle between the characteristic curves of the reduced equation (obtained by setting ε to zero in (1)) and the boundary [1]. Interior layers can appear, e.g., at interior discontinuities of $f(\mathbf{x})$, at singularities of the reduced equation, or along characteristics of the reduced equation.

Problem (1) has often been considered as a test case for numerical schemes. It is known that most numerical methods fail when the cell Reynolds number $v\,\Delta x/\varepsilon$ becomes $O(1)$. Here Δx is a typical mesh size and $v = \max_{\Omega(\mathbf{x})}(|V|)$.

The steps of our new algorithm are:

(i) The numerical solution of (1) is obtained on a fixed coarse grid with a special set of boundary conditions. This solution serves as a first approximation to the outer solution, u_o (see Section 3);

(ii) A set of one-dimensional boundary layer equations obtained from (1) are solved along the inner normal emanating from each point of Γ_b (see Section 5);

(iii) The outer solution, u_o, and the inner solution, u_i, are matched to obtain an approximate composite solution, u_A (see Section 4);

(iv) Correction terms are computed and added to the right-hand side of the discrete approximation of (1). This corrected discrete approximation is solved to obtain an improved solution, u_I (see Section 5);

(v) We replace u_A in (ii) by u_I and steps (ii)–(iv) are repeated until the new improved solution, u_I, agree with the approximate solution, u_A, to a specified tolerance (see Section 6).

In Section 7 we present numerical results for problems exhibiting interior or boundary layers.

3. OUTER SOLUTION

The outer solution, u_0, which is valid only far from boundary or interior layers is obtained by solving the differential equation (1) subject to the boundary conditions $u = U_g$ on Γ_g and suitable boundary conditions on Γ_b as described below. Following Kellogg and Tsan [13], it can be shown that the effect of the boundary conditions on Γ_b decays exponentially towards the interior of the domain. We chose the boundary conditions on Γ_b so that the outer solution has small gradients near Γ_b. This way it is possible to increase the numerical accuracy of the outer solution calculated on a given (typically coarse) mesh. The same argument is applied to interior layers: we replace continuity conditions on both sides of the interior layer with a set of conditions designed to reduce the effect of the layer on the overall solution. There are two possibilities for such boundary conditions as described below:

- "Natural boundary conditions" which are obtained from the weak formulation of the problem.
- "Improved outer boundary conditions" which are based on asymptotic arguments.

3.1. Boundary Layer Case

3.1.1. *Problem Definition*

Here the two possible formulations for an outer solution.

I. *Natural Boundary Conditions.* The outer solution satisfies Eqs. (1)–(2) and the boundary condition:

$$\mathbf{n} \cdot \nabla u = 0 \quad \text{on } \Gamma_b \tag{4}$$

which replaces (3). Here, $\mathbf{n}$ is the unit vector normal to Γ_b; Eq. (4) is naturally satisfied for a weak formulation of (1).

The exact solution of (1), (2), (4) converges to the exact solution of (1)–(3) far from Γ_b. It is possible to show that the magnitude of the gradient of the solution to (1), (2), (4) is smaller than the gradient of the typical solution to (1)–(3), by a factor of ε near Γ_b.

II. *Improved Outer Boundary Conditions.* Here the outer solution satisfies Eqs. (1)–(2) subject to the following "improved" outer boundary condition:

$$V_n \frac{\partial u}{\partial n} + au - f = 0 \quad \text{on } \Gamma_b, \tag{5}$$

where V_n is the component of V in the direction of the normal to Γ_b.

This boundary condition is derived using the following asymptotic argument. Assume that the outer solution can be expanded as

$$u_o(\mathbf{x}, \varepsilon) \sim \sum_{j=0}^{\infty} u_{oj} \varepsilon^j \tag{6}$$

and substituted into (1). To $O(\varepsilon)$, we obtain

$$\mathbf{V} \cdot \nabla u_{o\text{o}} + a u_{o\text{o}} = f \quad \text{in } \Omega \tag{7}$$

subject to

$$u_{o0} = U_g \quad \text{on } \Gamma_g. \tag{8}$$

If the solution to (1)–(3) is free of an interior layer, then the solution to (7)–(8) is smooth and satisfies (5) on Γ_b. The difference between the solution to (1)–(3) and u_{o0} is $O(\varepsilon)$ as $\varepsilon \to 0$ in the interior of Ω. Here we suggest solving Eq. (1) subject to (2) and to (7) to obtain a numerical approximation u_{o}. While the natural boundary condition (4) reduces the error of a numerical solution for u_{o} by a factor of ε, the "improved boundary condition" (5) reduces the same error by a factor ε^2.

The choice of boundary conditions is based on the accuracy of the inner solution. In general we would like to have a balanced scheme so that the accuracy of the inner and outer problems should be of the same order.

3.1.2. *Penalty Spectral Elements Formulation for u_o*

The solution of (1), (2), (4) is obtained numerically using a spectral method with a polynomial basis in each of the d-space dimensions. The calculated solution is smooth and converges to the exact solution far from the boundary layer when the polynomial degree of the approximate solution $N \to \infty$ for fixed ε.

A penalty spectral element formulation is used for the solution of the outer problem. The spectral element method [14] is chosen since the outer solution is expected to be smooth (without large gradients) and therefore this method can achieve an accurate outer solution with a small number of degrees of freedom.

We define the space $H^1(\Omega)$ to consist of all functions that are in $L^2(\Omega)$ and whose first derivatives are also in $L^2(\Omega)$. Applying the weighted residual method gives the following weak formulation to $u \in H^1_{E,\Gamma_g}(\Omega)$:

$$-\iint_\Omega \varepsilon \nabla w \cdot \nabla u \, d\Omega + \iint_\Omega w(\mathbf{V} \cdot \nabla u) \, d\Omega + \iint_\Omega awu \, d\Omega + \lambda \int_{\Gamma_b} w(u - U_b) \, d\Gamma_b = \int_\Omega wf \, d\Omega \quad \forall w \in H^1_{0,\Gamma_g}(\Omega). \tag{9}$$

Here w is the weighting function

$$H^1_{E,\Gamma_g}(\Omega) = \{v \in H^1(\Omega) | v(x) = U_g, \mathbf{x} \in \Gamma_g\}$$
$$H^1_{\mathrm{E},\Gamma_g}(\Omega) = \{v \in H^1(\Omega) | v(x) = 0, \mathbf{x} \in \Gamma_g\},$$

where the subscript E indicates that essential boundary conditions are applied on Γ_g. In (9), Dirichlet boundary conditions on Γ_b are imposed as penalty terms. When we solve the outer problem, we do not impose these conditions so λ is set to be zero. As a result, Neumann boundary conditions are naturally satisfied on Γ_b. We apply a penalty formulation in order to have the flexibility to use the same formulation (9) for both the outer solution ($\lambda = 0$) and for the improved solution (in which $\lambda \gg 1$) as will be shown in Section 6.

Applying a penalty spectral element approach to (9), we first specify a discretization pair $h = (n, \mathbf{N})$. The computational domain, Ω, is broken up into n macro-elements (spectral elements) so that $\Omega = \sum_{e=1}^{n} \Omega^e$. An approximate solution, u^h, is obtained by Lagrange interpolation of order $N = (N_x, N_y, N_z)$ with respect to $\mathbf{x}$. The space of u^h is taken to be the subspace X^h of H^1_{E,Γ_g} consisting of all piecewise high-order polynomials of degree $\leq \mathbf{N}$ with respect to $\mathbf{x}$ so that

$$X^h(\Omega) = \{\Phi \in H^0(\Omega), \Phi|_{\Omega^e} \in F_{\mathbf{N}}(\mathbf{x})\} \cap H^1_{E,\Gamma_g}(\Omega). \tag{10}$$

The spectral element formulation is

$$-\iint_\Omega \varepsilon \nabla w^h \cdot \nabla u^h \, d\Omega + \iint_\Omega w^h(\mathbf{V} \cdot \nabla u^h) \, d\Omega + \iint_\Omega aw^h u^h \, d\Omega^e + \lambda \int_{\Gamma_b} w^h(u^h - U_b) \, dT_b = \int_\Omega w^h f \, d\Omega \quad \forall w^h \in Z^h. \tag{11}$$

Here with w^h lies in the subspace Z^h so that

$$Z^h(\Omega) = \{\Phi \in H^0(\Omega), \Phi|_{\Omega^e} \in F_{\mathbf{N}}(\mathbf{x})\} \cap H^1_{0,\Gamma_g}(\Omega). \tag{12}$$

The integrations in (11) done using Gauss–Lobatto–Legendre quadrature leading to a set of algebraic equations.

3.2. Interior Layer Case

Let us assume for simplicity that we consider the case in which $f(\mathbf{x})$ is piecewise continuous with jumps along a surface Σ trying in Ω. The choice of boundary conditions on the outer solution is as follows.

3.2.1. *Problem Definition*

I. *Natural Boundary Conditions on* Σ. Here we apply

$$\mathbf{n} \cdot \nabla u = 0 \tag{13}$$

on each side of the surface Σ.

II. *Improved Boundary Conditions on* Σ. Here the differential equation (1) is approximated on Σ by dropping the term proportional to ε (assuming that ε is small). The resulting improved boundary condition is

$$\mathbf{V} \cdot \nabla u + au = f \tag{14}$$

on each side of Σ.

3.2.2. *Penalty Spectral Element Formulation*

The spectral element formulation for Eqs. (1), (2), subject to (13) or to (14), is similar to the one obtained for the boundary layer problem (see Section 3). Here, in order to obtain Neumann boundary conditions on Σ, λ should equal zero. The outer solution is discontinuous across Σ so that $[u(\mathbf{x})]_\Sigma \neq 0$. In this case, the spectral elements weighting function w^h should also be discontinuous across Σ so that $[w^h(\mathbf{x})]_\Sigma \neq 0$. Under these conditions the spectral element formulation is a straightforward variant of the boundary layer spectral element formulation.

As in the boundary layer formulation, large λ forces continuity for the solution u and for the normal derivative, $\mathbf{n} \cdot \nabla u$, on Σ.

The penalty method as presented here is more efficient for the numerical treatment of interior layers than a standard spectral element method. In the latter case, additional assembly is required, while in the present approach the same spectral element matrices are needed for both the outer and the improved solutions. These matrices only differ by the terms which are multiplied by λ.

4. INNER SOLUTION

The outer solution is valid only far from Γ_b or Σ and, thus, should be corrected by an inner solution, u_i, which is valid near these surfaces. That is, we seek an asymptotic approximation u_{i} to $u - u_{\mathrm{o}}$. In order to investigate the solution in the neighborhood of Γ_b or Σ we first employ a coordinate transformation $\mathbf{x} = (x, y) \to (\xi, \eta)$. Here, for simplicity, we assume that $d = 2$. For a point $\mathbf{x}$ close to Γ_b or Σ, let us define a coordinate system (ξ, η) originating on the boundary point $\mathbf{x}_0$ that lies closest to $\mathbf{x}$. Let η be the coordinate tangential to this boundary and let ξ be a stretched variable in the direction normal to the boundary. The transformation $(\mathbf{x}) \to (\xi, \eta)$ for $\Omega \subset \mathscr{R}^2$ is given locally near Γ_b or Σ by

$$\mathbf{x}(\xi, \eta) = \mathbf{x}_o + \varepsilon\xi\mathbf{n}, \tag{15}$$

where $\mathbf{n} = [-(\partial y_o/\partial\eta)/(\partial x_o/\partial\eta)]$ is the unit normal at $\mathbf{x}_0$. The inner solution, u_{i}, is obtained by substituting the asymptotic expansion:

$$u_{\mathrm{i}}(\xi, \eta; \varepsilon) = \sum_{n=0}^{\infty} u_{in}(\xi, \eta)\varepsilon^n \tag{16}$$

into (1) and equating the leading-order terms. Outside corner regions, we then obtain a one-dimensional second-order differential equation in the local coordinate ξ.

Near a boundary layer, the inner solution, u_{i}, should satisfy the boundary conditions:

$$\begin{aligned} u_{\mathrm{i}}(\xi = 0, \eta) &= U_b(\eta) - u_{\mathrm{o}}(\xi = 0, \eta) \\ u_{\mathrm{i}}(\xi \to \infty, \eta) &= 0 \quad \forall\eta \in \Gamma_b. \end{aligned} \tag{17}$$

And near an interior layer

$$\begin{aligned} u_{\mathrm{i}}(\xi = 0^{(-)}, \eta) + u_{\mathrm{o}}(\xi = 0^{(-)}, \eta) &= u_{\mathrm{i}}(\xi = 0^{(+)}, \eta) + u_{\mathrm{o}}(\xi = 0^{(+)}, \eta) \\ u_{\mathrm{i}}(\xi \to \pm\infty, \eta) &= 0 \quad \forall\eta \in \Sigma. \end{aligned} \tag{18}$$

The values for u_{o} in (18) are taken from the outer solution process which was obtained according to Section 3.

These one-dimensional problems are defined for each η on the boundary. They are to be solved along rays orthogonal to the boundary Γ_b or Σ and originating at grid points lying on these boundaries.

The resulting inner solution gives the approximate solution

$$u_A(\mathbf{x}; \varepsilon) = u_{\mathrm{o}}(\mathbf{x}) + u_{\mathrm{i}}(\xi(\mathbf{x}), \eta(\mathbf{x})) \tag{19}$$

which is an $O(\varepsilon)$ approximation through Ω.

If there is a corner in Γ_b, the inner problem cannot be reduced to a one-dimensional problem in the vicinity of this corner. For simplicity, let us assume a two-

dimensional domain with one corner in Γ_b which is located at the origin of the $x - y$ coordinate system and that its two edges coincide with the x and y directions, respectively. The values of the outer solution near the corner are updated twice: first, after the computation of the x-boundary layer, and then after the computation of the y-boundary layer. This second update mostly affects the solution in the corner where the x and y boundary layers meet. The extension to three-dimensional problems is then straightforward. A more accurate procedure, albeit more expensive, is to use a multidimensional inner solution in corners.

5. IMPROVED SOLUTION

The ''booster method,'' introduced by Israeli and Ungarish [5], exploits analytic asymptotic approximations (or possibly other approximation methods) to obtain an accurate global approximation to the solution of a partial differential equation on a coarse grid. The method is summarized as follows.

For a linear partial differential equation,

$$L(u) = f \quad \text{in } \Omega, \tag{20}$$

subjected to appropriate boundary conditions, a numerical solution u_n is usually obtained directly from

$$L_h(u_n) = f_h \quad \text{in } \Omega, \tag{21}$$

where L_h and f_h are the discretized approximations for L and f. Instead, in the ''booster method,'' we use an approximate analytic solution, u_A of (20) to obtain an improved solution u_I from

$$L_h(u_I) = L_h(u_A) - L(u_A) + f_h \quad \text{in } \Omega. \tag{22}$$

The error of the improved solution, e_I, obtained by the booster method can be estimated by (see [5])

$$\|e_I\|_j \approx c_j \|e_n\|_j \cdot \|e_A\|_j, \quad j = 0 \cdots \infty, \tag{23}$$

where e_n denotes the error of a numerical solution of the problem and e_A is the error of the approximate solution.

The discretized approximations L_h and f_h are calculated according to the penalty-spectral element formulations as described in Section 4. Here λ is set to be large enough. In order to estimate its value for the case of an interior layer problem, we should first rewrite the continuity condition across Σ. Instead of satisfying the continuity condition, the following condition is valid across Σ:

$$\lambda[u(\mathbf{x})] = \mathbf{n} \cdot \nabla u \quad \text{on } \sum \tag{24}$$

which is a weak form of the continuity condition. The normal derivative $\mathbf{n} \cdot \nabla u(\mathbf{x})$ on Σ can be written as a function of the stretched, normal to $\mathbf{n}$, coordinate ξ so that

$$\mathbf{n} \cdot \nabla u(\mathbf{x}) = \frac{1}{\varepsilon} \frac{\partial u}{\partial \xi} \quad \text{on } \sum \tag{25}$$

and thus the continuity requirements for the solution are related to

$$[u(\mathbf{x})] \approx \frac{1}{\lambda \varepsilon} \frac{\partial u}{\partial \xi} \quad \text{on } \sum, \tag{26}$$

where the value of $\partial u / \partial \xi$ is of $O(1)$ if ε is of the order of the layer width.

6. SUMMARY OF THE ALGORITHM

6.1. Steps of the Algorithm

The algorithm proposed here is summarized as follows:

1. The outer solution, u_0, to (1) is obtained numerically on a coarse grid using (11) and letting λ tend to zero.

2. The inner solution, u_i, is obtained analytically according to Section 5.

3. The two solutions, u_0 and u_i, are matched according to (32) to obtain an "analytic" approximation, u_A, to the exact solution (32).

4. Equation (22) is solved (on a coarse grid) using an appropriate choice for λ.

5. The outer part of u_I is substituted into u_A and step 2 is repeated until convergence is attained. The outer part of u_I is calculated by subtraction of u_{i} from u_I.

6.2. Interpolated Solution

The numerical solution, $\mathbf{u}_I$, is a discrete solution calculated at the nodal points of the elemental grid. Intermediate values for the solution, $u_I(\mathbf{x})$, cannot be obtained by direct interpolation using the spectral element basis since the solution does not belong to the space spanned by this basis [11]. Let us first write the matrix form of (22) as

$$\mathbf{K}\mathbf{u}_I = \mathbf{f} + (\mathbf{K}\mathbf{u}_A - \mathbf{f}^A), \tag{27}$$

where $\mathbf{K}$ and $\mathbf{f}$ are the stiffness matrix and right-hand vector respectively obtained from the spectral elements formulation of (1)–(3). The vector $\mathbf{f}^A$ equals $L(\mathbf{U}_A)$. Or alternatively,

$$\mathbf{K}(\mathbf{u}_I - \mathbf{u}_A + \mathbf{K}^{-1}\mathbf{f}^A) = \mathbf{f}. \tag{28}$$

If we define

$$\mathbf{u}_m = (\mathbf{u}_I - u_A + \mathbf{K}^{-1}\mathbf{f}^A) \tag{29}$$

then

$$\mathbf{K}\mathbf{u}_m = \mathbf{f}. \tag{30}$$

The function $u_m(\mathbf{x})$ satisfies (30) and, thus, belongs to the space spanned by the spectral element basis. Therefore $u_m(\mathbf{x})$ can be expressed as

$$u_m(\mathbf{x}) = I_N(\mathbf{u}_m), \tag{31}$$

where I_N is the spectral-element interpolation operator based on Legendre–Gauss–Lobatto points. The analytical approximation is composed of the numerical outer solution, $\mathbf{u}_o$, and the analytical inner solution, $u_i(\xi(\mathbf{x})\eta(\mathbf{x})$, so

$$\begin{aligned} u_A(\mathbf{x}) &= u_{\mathrm{o}}(\mathbf{x}) + u_{\mathrm{i}}(\xi(\mathbf{x}), \eta(\mathbf{x})) \\ &= I_N(\mathbf{u}_{\mathrm{o}}) + u_{\mathrm{i}}(\xi(\mathbf{x}), \eta(\mathbf{x})). \end{aligned} \tag{32}$$

The inner solution, u_{i}, is analytical and continuous in $\xi(\mathbf{x})$ but it is discrete in $\eta(\mathbf{x})$. As a result we can write for each discrete point η_n an analytical solution $u_{\mathrm{i}}(\xi, \eta_n)$. The inner solution at $\eta \neq \eta_n$ can be calculated by a one-dimensional Lagrange interpolation formula of order N. That is because of the restriction that the variation of the inner solution in the η direction is determined by the outer solution which is spanned by the spectral element basis.

If we introduce the booster term

$$\mathbf{u}_r = \mathbf{K}^{-1}\mathbf{f}^A \tag{33}$$

with

$$u_r(\mathbf{x}) = I_N(\mathbf{u}_r). \tag{34}$$

Then, the improved solution u_I is expressed as

$$\begin{aligned} u_I(\mathbf{x}) &= I_N(\mathbf{u}_o) + u_{\mathrm{i}}(\xi(\mathbf{x})) + I_N(\mathbf{K}^{-1}\mathbf{f}^A) \\ &= I_N(\mathbf{u}_o + \mathbf{K}^{-1}\mathbf{f}^A) + u_{\mathrm{i}}(\xi(\mathbf{x})). \end{aligned} \tag{35}$$

7. NUMERICAL EXAMPLES

7.1. Two-Dimensional Problem with a Boundary Layer

Here we apply the method described above to the two-dimensional convection-diffusion problem:

$$\begin{aligned} \varepsilon\nabla^2 u + \mathbf{V}\cdot\nabla u = 0 \quad \mathbf{x} \in (0,1)^2 \\ u(x,0) = 0 \\ u(x,1) = \sqrt{x} \\ u(0,y) = 0 \\ u(1,y) = \sqrt{y}, \end{aligned} \tag{36}$$

where $\mathbf{V} = (1, 1)$.

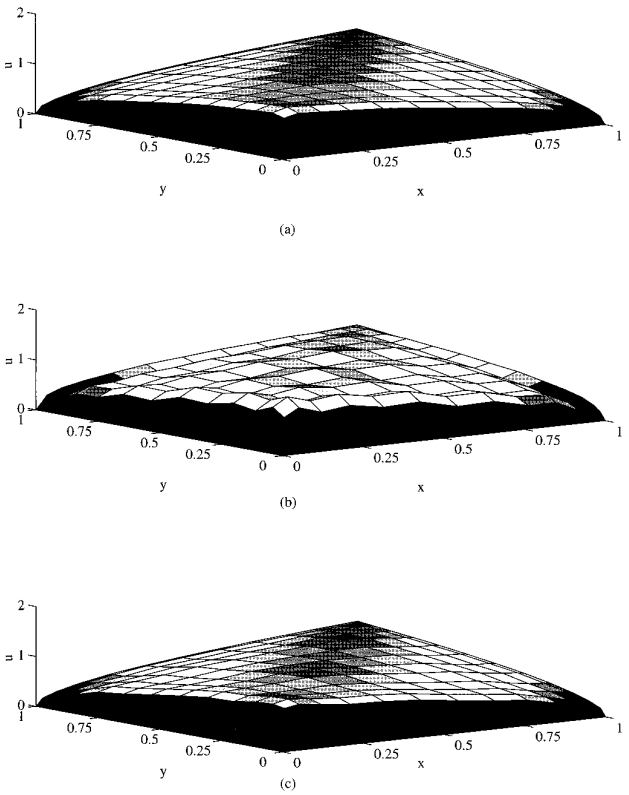

FIG. 1. Solution for a two-dimensional problem ($\varepsilon = 8 \times 10^{-3}$): (a) Reference (high resolution) solution; (b) Numerical (spectral) solution u_n, $N = 13$; (c) Improved solution u_I, $N = 13$.

For this problem we seek a solution composed of an outer solution, u_{o}, and an inner solution, u_{i}, as follows:

$$u_A(\mathbf{x}; \varepsilon) = u_{\mathrm{o}}(\mathbf{x}) + \sum_{n=o}^{\infty} (u_{in}\varepsilon^n. \tag{37}$$

The solution for u_{o} is two-dimensional and is computed as described in Sections 3–4. For the inner solution (setting $n = 0$ in (37)) the following one-dimensional differential equation must be solved in the direction normal to Γ_b:

$$\frac{d^2u_{\mathrm{i}}}{d\xi^2} + \frac{du_{\mathrm{i}}}{d\xi} = 0 \quad \forall \eta \in \Gamma_b \tag{38}$$

The solution to (38), is subject to the boundary conditions (17), is:

$$u_i(\xi, \eta) = U_b(\eta) - u_o(\xi = 0, \eta)]e^{-\xi} \quad \forall \eta \in \Gamma_b \tag{39}$$

and the approximate solution, u_A, is

$$u_A(\mathbf{x}) = u_{\mathrm{o}}(\mathbf{x}) + [U_b(\eta) - u_{\mathrm{o}}(\xi = \mathrm{o}, \eta)]e^{-\xi} \quad \forall \eta \in \Gamma_b. \tag{40}$$

In Fig. 1a we plot a reference solution of (36), obtained by numerical solution

of (36) on a very fine grid. In contrast, the results for a coarse numerical solution, u_n, using one spectral element of order $N_x = N_y = 13$, are plotted in Fig. 1b. The latter solution oscillates throughout the domain. Increasing the number of elements with fixed N_x, N_y leads to smaller wiggles in the solution because of the reduced coupling between the elements as compared with a fully spectral solution. In Fig. 1c we plot the improved solution u_I obtained using the same coarse grid mesh ($N_x = N_y = 13$) as for the fully spectral solution u_n. The error distribution arising from the fully numerical solution, u_n, and from the different stages of the solution are presented in Figs. 2a–d. The error of the numerical solution is $\|e_n\|_\infty = 0.13$ (Fig. 2a). The error of the present solution after the first analytical correction (obtained on the edge $x = 0$) is still large on the boundary (the edge $y = 0$) on which the correction has not yet been performed (Fig. 2b). As expected, the error norm after the correction on all boundaries (Fig. 2c) attains its maximum value near the corners ($\|e_a\|_\infty = 0.17$). Using the mixed analytical numerical procedure (22) leads to a final solution with error norm $\|e_I\|_\infty = 4\ 10^{-2}$ (Fig. 2d).

In order to show the efficiency of the present solution, we define a ratio which is based on (23) as follows:

$$\kappa = \frac{\|e_I\|_\infty}{\|e_n\|_\infty \cdot \|e_A\|_\infty}. \tag{41}$$

The value of κ was estimated for various polynomial degrees and several values of ε. The boundary conditions were chosen so that an analytical reference solution can be found. The results for k are summarized in Table I.

For all the values of N and ε considered here, k is found to be $O(1)$. For sufficiently small values of ε, the method shows an improvement over the fully numerical method. The approximate solution is weakly affected by the polynomial degree of the outer solution since the error e_A is composed of the error of the numerical outer solution and the error of the inner analytical solution, which is dominant.

The efficiency of the improved solution compared to a fully numerical solution can be evaluated using the results plotted in Fig. 3. We assume that the number of operations which are needed for a numerical solution is of order of p^3, where p is the total number of degrees of freedom. For $\varepsilon = 3 \times 10^{-3}$ and $N = 11$ the error obtained from the improved solution is $\|e_I\|_\infty = 1.69 \times 10^{-2}$. In order to get a numerical error similar to the error of the improved solution, the polynomial degree of the spectral solution would have to be increased to $N \approx 35$ (see Fig. 3) (even with the highly efficient boundary layer resolution of such a polynomial spectral method). This result means that the ratio, $Ef(\varepsilon)$, between the number of operations for the two solutions is

$$Ef(0.003) \approx \left(\frac{35^2}{2\ 11^2}\right)^3 \approx 130 \tag{42}$$

and for $\varepsilon = 0.005$ (see Fig. 3),

$$Ef(0.005) \approx \left(\frac{25^2}{2\ 11^2}\right)^3 \approx 20. \tag{43}$$

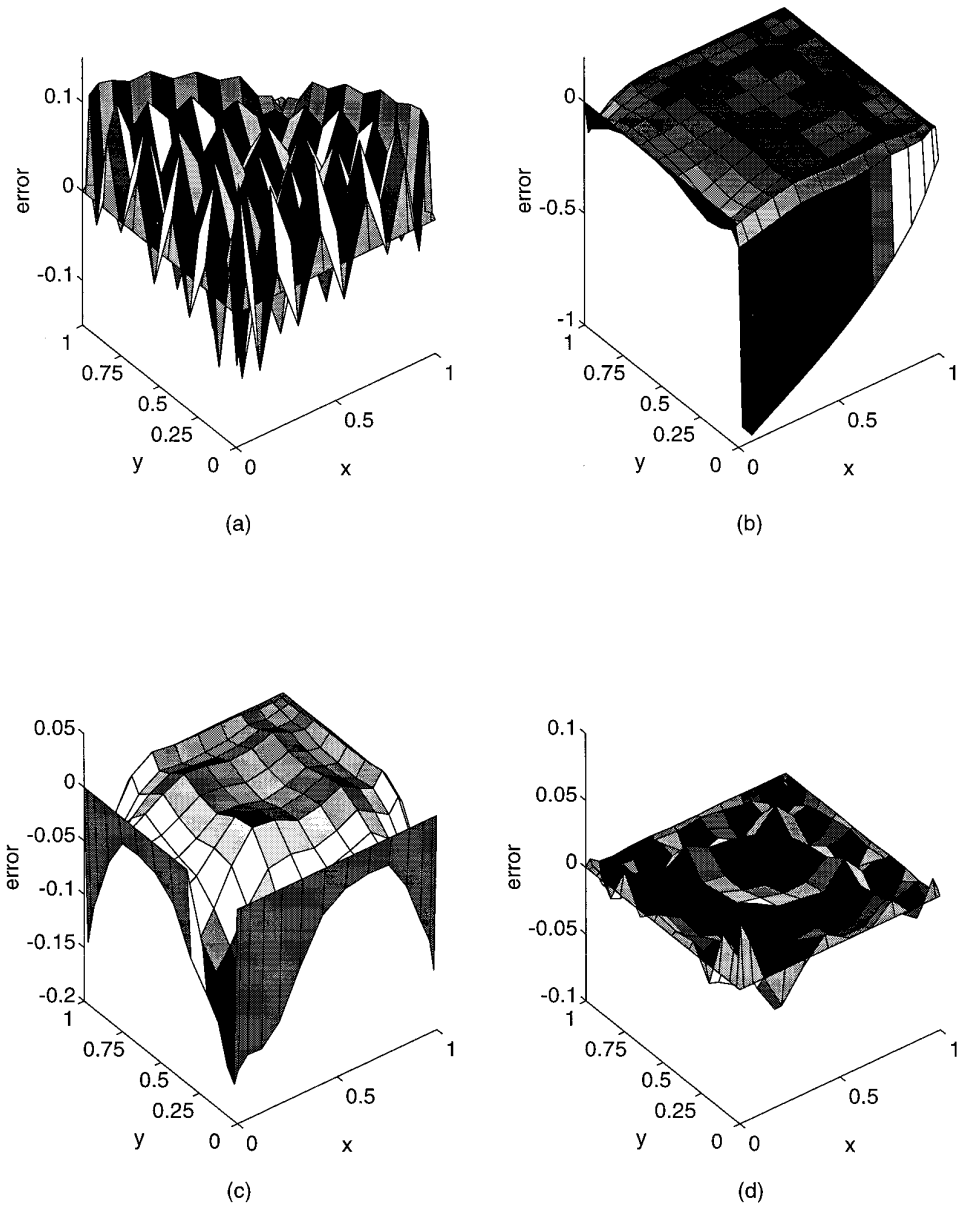

FIG. 2. Error distribution ($\varepsilon = 8 \times 10^{-3}$): (a) Numerical solution $\|e_n\|_\infty = 0.13$; (b) First correction $\|e\|_\infty = 0.97$; (c) Second correction $\|e_A\|_\infty = 0.17$; (d) Improved solution $\|e_I\|_\infty = 4 \times 10^{-2}$.

The algorithm was also applied to problems with different values of ε in the x and y directions of Ω. If the value of ε is high enough in one of the directions the correction could be done only for the second direction in which ε is small (see Figs. 4, 5). In this case the source of the wiggles is from the x direction so that there is no need to correct the solution in the vicinity of the y boundary.

When $a \neq 0$ in (1) and the velocity of the advection term is parallel to the boundary ($\mathbf{V} = [1, 0]$) two types of boundary layers are present: one of order ε

TABLE I
Errors of the Different Procedures (2D Case)

$N \Downarrow$	$\varepsilon \Rightarrow$	0.01	0.008	0.005	0.003
11	$\|e_n\|_\infty$	3.50×10^{-1}	5.40×10^{-1}	1.14×10^{0}	2.19×10^{0}
	$\|e_A\|_\infty$	3.31×10^{-1}	1.74×10^{-1}	8.29×10^{-2}	3.10×10^{-2}
	$\|e_I\|_\infty$	3.55×10^{-2}	2.49×10^{-2}	2.38×10^{-2}	1.69×10^{-2}
	κ	0.306	0.265	0.251	0.248
14	$\|e_n\|_\infty$	1.01×10^{-1}	1.61×10^{-1}	3.29×10^{-1}	5.04×10^{-1}
	$\|e_A\|_\infty$	3.30×10^{-1}	1.72×10^{-1}	8.25×10^{-2}	3.11×10^{-2}
	$\|e_I\|_\infty$	1.10×10^{-2}	9.20×10^{-3}	1.21×10^{-2}	5.13×10^{-3}
	κ	0.33	0.33	0.44	0.32
16	$\|e_n\|_\infty$	4.80×10^{-2}	8.80×10^{-2}	2.20×10^{-1}	4.00×10^{-1}
	$\|e_A\|_\infty$	3.1×10^{-1}	1.74×10^{-1}	8.22×10^{-2}	3.09×10^{-2}
	$\|e_I\|_\infty$	1.80×10^{-2}	6.43×10^{-3}	6.15×10^{-3}	4.8×10^{-3}
	κ	1.21	0.42	0.34	0.38
18	$\|e_n\|_\infty$	2.03×10^{-2}	6.00×10^{-2}	1.46×10^{-1}	3.17×10^{-1}
	$\|e_A\|_\infty$	3.02×10^{-1}	1.69×10^{-1}	8.11×10^{-2}	2.99×10^{-2}
	$\|e_I\|_\infty$	1.73×10^{-2}	5.03×10^{-3}	3.12×10^{-3}	2.52×10^{-3}
	κ	2.85	0.49	0.26	0.27

and a second one of order $\sqrt{\varepsilon}$. In such a case we often need to improve only the solution near the boundary layer of order ε. In Fig. 6 we present the results for a test problem: the reference numerical solution is shown in Fig. 6a. A fully numerical spectral solution based on a low order polynomial approximation ($N = 13$) produces

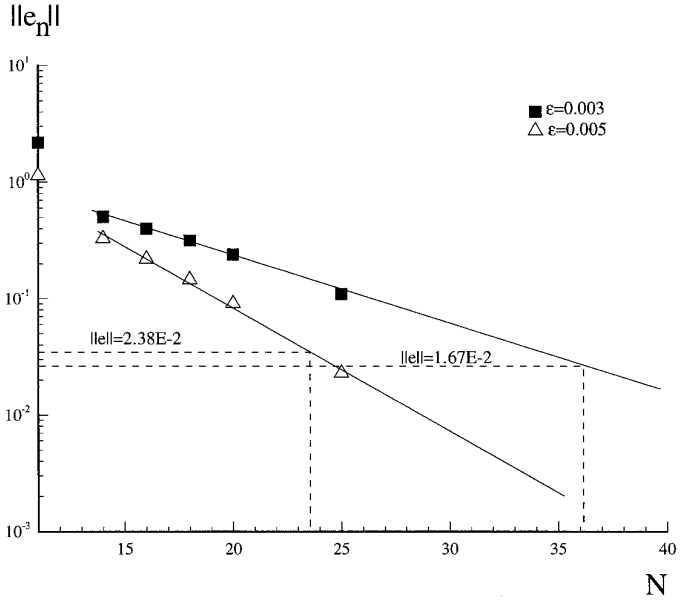

FIG. 3. Efficiency of the improved solution.

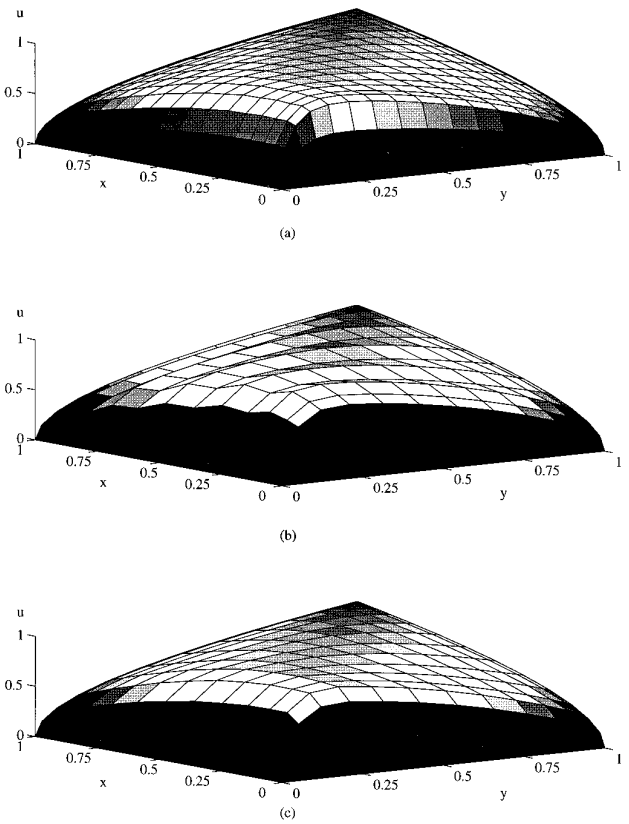

FIG. 4. A two-dimensional problem with anisotropic ε ($\varepsilon_x = 1 \times 10^{-2}$, $\varepsilon_y = 5 \times 10^{-2}$): (a) Reference solution; (b) Numerical (spectral) solution u_n, $N = 13$; (c) Improved solution u_I, $N = 13$.

a large oscillatory error because of the x direction boundary layer [$0(\varepsilon)$]. The calculated outer solution, u_0, is presented in Fig. 6c and is free of oscillations. The hybrid solution can be calculated by matching this solution with a one-dimensional solution, u_{i} (Fig. 6d). This solution is much more accurate than the fully numerical solution which is based on the same coarse grid (Figs. 6e, f).

7.2. One-Dimensional Problem with an Interior Layer

The present algorithm can be applied to the solution of problems having interior layers. To illustrate this, let us consider the following one-dimensional problem:

$$\varepsilon^2 u_{xx} - u = -f(x), \quad x \in (-0.5, 0.5). \tag{44}$$

The outer solution for this equation is calculated numerically as in Sections 3, 4 and the inner solution, $u_{\mathrm{i}}(\xi)$, should satisfy the equation:

$$\frac{d^2 u_i}{d\xi^2} - u_i = u_o - f, \quad \xi \in \left[\frac{-x_1}{\varepsilon}, \frac{1 - x_1}{\varepsilon}\right], \tag{45}$$

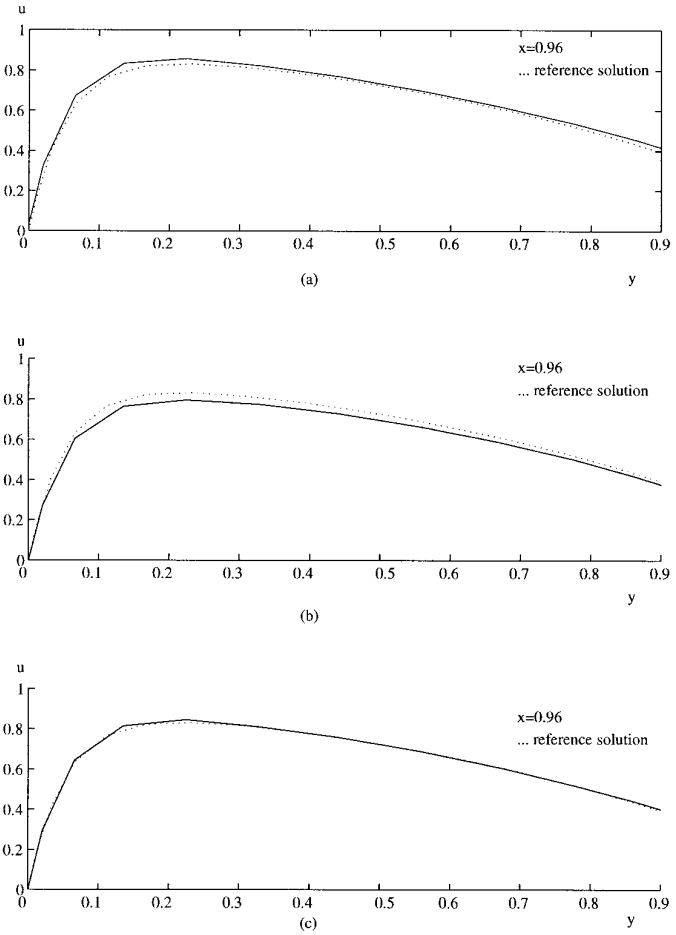

FIG. 5. The effect of various options at a fixed x coordinate ($x = 0.92$): (a) Analytical correction $\|e_A\|_\infty = 0.184$; (b) Numerical solution $\|e_n\|_\infty = 0.131$; (c) Improved solution $\|e_I\|_\infty = 4.9 \times 10^{-2}$.

where x_1 is the location of the interior layer and $\xi = (x - x_1 + 0.5)/\varepsilon$. For the inner problem it is convenient to use $f(x)$ as an approximation for u_o, since the difference between them is of $O(\varepsilon)$. The solution for (45) is

$$\begin{aligned} u_i^{(-)}(\xi) &= Ae^{\xi} + Be^{-\xi}, \quad \xi \le 0, \\ u_i^{(+)}(\xi) &= De^{\xi} + Ee^{-\xi}, \quad \xi \ge 0. \end{aligned} \tag{46}$$

The solutions to both equations should satisfy the conditions that $u_i = 0$ for $\xi \to \infty$ so that

$$\begin{aligned} u_i^{(-)}(\xi) &= Ae^{\xi}, \quad \xi \le 0, \\ u_i^{(+)}(\xi) &= Ee^{-\xi}, \quad \xi \ge 0. \end{aligned} \tag{47}$$

The coefficients A and E are evaluated after applying continuity conditions to both the solution, u_A, and its derivative so that

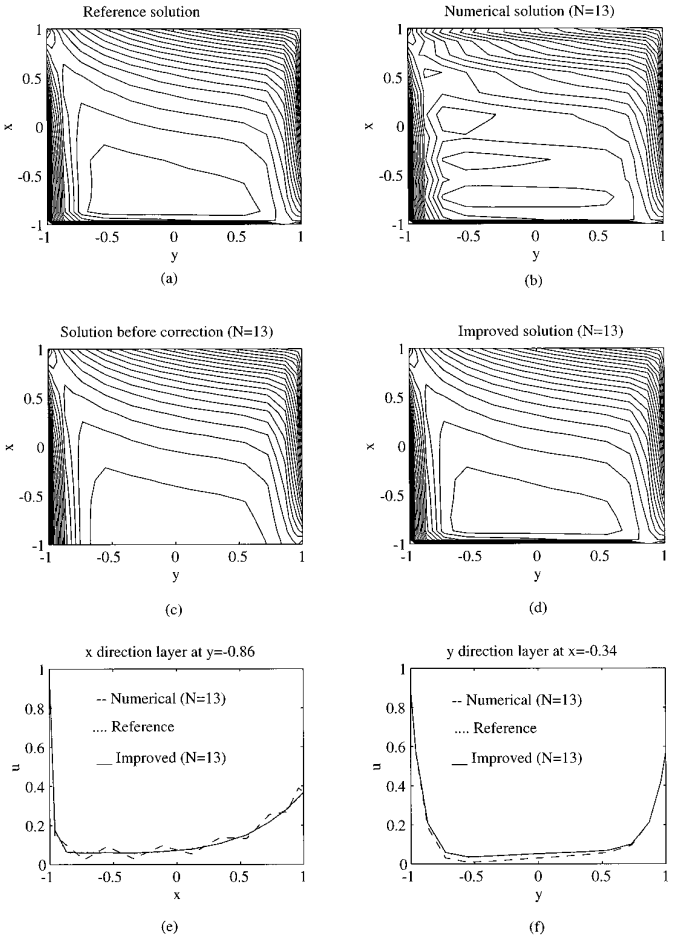

FIG. 6. Solution of a two-dimensional problem with different types of boundary layer ($\varepsilon_x = \varepsilon_y = 5 \times 10^{-3}$; $a = -4$; $v = [1, 0]$): (a) Reference solution; (b) Numerical (spectral) solution u_n, $N = 13$; (c) Outer solution u_o, $N = 13$; (d) Improved solution u_I, $N = 13$; (e) Comparison between the different solutions in the x direction on a fixed line $y = -0.86$; (f) Comparison between the different solutions in the y direction on a fixed line $x = -0.34$.

$$2A = u_o^{(+)}(x_t) - u_o^{(-)}(x_t) + \varepsilon \left(\frac{du_o^{(+)}(x_t)}{dx} - \frac{du_o^{(-)}(x_t)}{dx} \right.$$
$$2E = -u_o^{(+)}(x_t) - u_o^{(-)}(x_t) + \varepsilon \left(\frac{du_o^{(+)}(x_t)}{dx} - \frac{du_o^{(-)}(x_t)}{dx} \right). \tag{48}$$

As a first example we will consider the case where $f(x)$ is discontinuous at $x_1 = 0.5$,

$$f(x) = \begin{cases} (4x-1)^2, & \text{if } 0 \le x < 0.5, \\ -(4x-1)^2, & \text{if } 0.5 < x \le 1. \end{cases}$$

TABLE II
Errors of the Different Procedures for Discontinuous $f(x)$

$N \Downarrow$	$\varepsilon^2 \Rightarrow$	2×10^{-5}	1×10^{-5}	5×10^{-6}	2×10^{-6}
10	$\|e_n\|_\infty$	2.97×10^{-2}	2.31×10^{-2}	1.42×10^{-2}	5.93×10^{-3}
	$\|e_A\|_\infty$	6.40×10^{-4}	3.20×10^{-4}	1.64×10^{-4}	6.40×10^{-5}
	$\|e_I\|_\infty$	1.29×10^{-5}	9.15×10^{-6}	1.37×10^{-6}	2.39×10^{-7}
	κ	0.68	0.67	0.61	0.63
11	$\|e_n\|_\infty$	2.96×10^{-2}	2.73×10^{-2}	1.86×10^{-2}	8.39×10^{-3}
	$\|e_A\|_\infty$	6.40×10^{-4}	3.20×10^{-4}	1.64×10^{-4}	6.37×10^{-5}
	$\|e_I\|_\infty$	1.76×10^{-5}	6.99×10^{-6}	2.20×10^{-6}	4.12×10^{-7}
	κ	0.92	0.81	0.74	1.00
13	$\|e_n\|_\infty$	2.28×10^{-2}	2.96×10^{-2}	2.66×10^{-2}	1.49×10^{-2}
	$\|e_A\|_\infty$	6.40×10^{-4}	3.20×10^{-4}	1.64×10^{-4}	6.40×10^{-5}
	$\|e_I\|_\infty$	2.31×10^{-5}	1.29×10^{-5}	4.83×10^{-6}	9.97×10^{-7}
	κ	1.50	1.37	1.12	1.04
15	$\|e_n\|_\infty$	1.35×10^{-2}	2.48×10^{-2}	2.97×10^{-2}	2.22×10^{-2}
	$\|e_A\|_\infty$	6.40×10^{-4}	3.20×10^{-4}	1.64×10^{-4}	6.40×10^{-5}
	$\|e_I\|_\infty$	2.85×10^{-5}	1.77×10^{-5}	8.44×10^{-6}	1.72×10^{-6}
	κ	3.2	2.26	1.76	1.40

In Table II we present the maximal error at nodal points for different values of the polynomial degree, N, and ε. For the particular differential equation under consideration the numerical solution does not produce wiggles for low values of ε (Fig. 6) because it converges to a solution of linear algebraic equations for $\varepsilon \to 0$. When the first derivative of u was present in the equation, the numerical solution was less accurate and much more oscillatory (like the two-dimensional boundary layer case). A plot of the different steps of the solution is presented in Fig. 7 for the case $\varepsilon = 2 \times 10^{-5}$ and $N = 15$. The inner solution is discontinuous and decays to zero far from the boundary layer. Our final example is the case where $f(x)$ is chosen so that it is continuous within the domain but has a discontinuous derivative at some point within the domain. We choose $f(x) = |x - 0.5|$ so that

$$u_o^{(-)}(x_t) = u_o^{(+)}(x_t)$$
$$\frac{du_o^{(-)}(x_t)}{dx} = -\frac{du_o^{(+)}(x_t)}{dx} = O(1). \tag{49}$$

For this problem the solution u_A is

$$u_A = u_o + O(\varepsilon)e^{-|\xi|}. \tag{50}$$

From Table III we can see that for this example the improved solution is much more accurate than both the numerical and analytical approximations. As shown in (27) the numerical and the analytical approximations are of the same order for low values of ε. For such problems it may be worthwhile to improve the results by

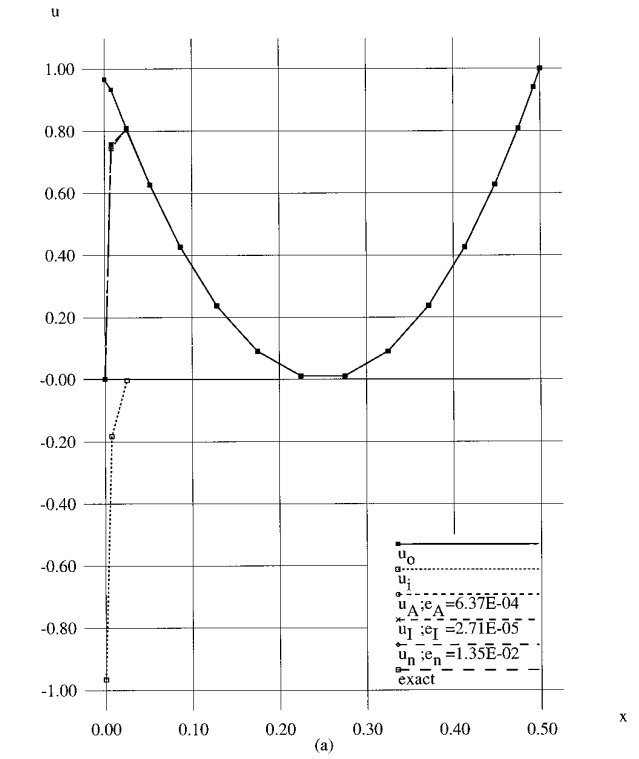

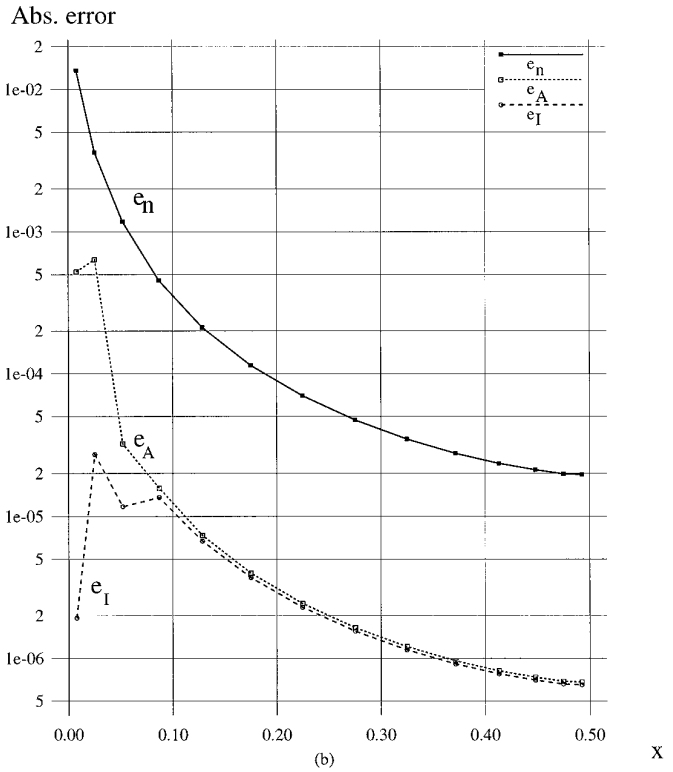

FIG. 7. The solution with range $0 \leq x \leq 0.5$ ($\varepsilon = 2 \times 10^{-5}$, $N = 15$): (a) Different stages of the solution; (b) Error distribution.

TABLE III
Comparison between the Various Stages of the Solution and a Numerical Solution for Discontinuous $df(x)/dx$

$N \Downarrow$	$\varepsilon^2 \Rightarrow$	1×10^{-5}	5×10^{-6}	2×10^{-6}	1×10^{-6}	7×10^{-7}
11	$\|e_n\|_\infty$	0.399	0.544	0.698	0.783	0.818
	$\|e_A\|_\infty$	0.400	0.345	0.254	0.192	0.165
	$\|e_I\|_\infty$	8.0×10^{-2}	5.9×10^{-2}	3.38×10^{-2}	2.26×10^{-2}	2.24×10^{-2}
	κ	0.5	0.314	0.19	0.15	0.17
12	$\|e_n\|_\infty$	0.317	0.470	0.643	0.742	0.787
	$\|e_A\|_\infty$	0.413	0.377	0.291	0.224	0.193
	$\|e_I\|_\infty$	8.5×10^{-2}	7.23×10^{-2}	4.3×10^{-2}	3.25×10^{-2}	3.28×10^{-2}
	κ	0.65	0.407	0.230	0.196	0.22
14	$\|e_n\|_\infty$	0.182	0.328	0.526	0.651	0.704
	$\|e_A\|_\infty$	0.393	0.412	0.354	0.285	0.250
	$\|e_I\|_\infty$	7.7×10^{-2}	8.5×10^{-2}	6.32×10^{-2}	6.08×10^{-2}	6.36×10^{-2}
	κ	1.07	0.629	0.339	0.32	0.36
18	$\|e_n\|_\infty$	4.14×10^{-2}	0.127	0.301	0.454	0.528
	$\|e_A\|_\infty$	0.24	0.356	0.414	0.383	0.353
	$\|e_I\|_\infty$	2.98×10^{-2}	6.33×10^{-2}	8.4×10^{-2}	7.1×10^{-2}	2.56×10^{-2}
	κ	2.95	1.45	0.67	0.4	0.17

using a ''mixed'' numerical solution. Instead of solving for the original differential equation (see (21)) two new variables (u and the derivative of u) can be defined. The correction can then be computed only for the derivative of u.

7.3. Two-Dimensional Problem with Boundary and Interior Layers

As a final example we consider

$$\varepsilon \nabla^2 u - u = f, \quad \mathbf{x} \in (0, 1)^2, \tag{51}$$

subject to Dirichlet boundary conditions,

$$\begin{aligned} u &= 5 \quad \text{on } \Gamma_1 \\ u &= 1 \quad \text{on } \Gamma_2. \end{aligned} \tag{52}$$

The domain Ω is divided by Σ into two subdomains Ω_1 and Ω_2 so that $\Omega = \Sigma \cup \Omega_1 \cup \Omega_2$ (Fig. 8) and the source function:

$$f(\mathbf{x}) = \begin{cases} x^3 + y^3 & \text{on } \mathbf{x} \in \Omega_1 \\ -(x^3 + y^3) & \text{on } \mathbf{x} \in \Omega_2. \end{cases}$$

The solution for (51)–(52) exhibit boundary layers near Γ_1 and Γ_2 and an interior layer near Σ. Our outer solution, u_0, satisfy Eq. (51). It is discontinuous in Σ and as a result is calculated separately in each of the subdomains Ω_1 and Ω_2. The outer solution in Ω_1 is subject to the boundary conditions

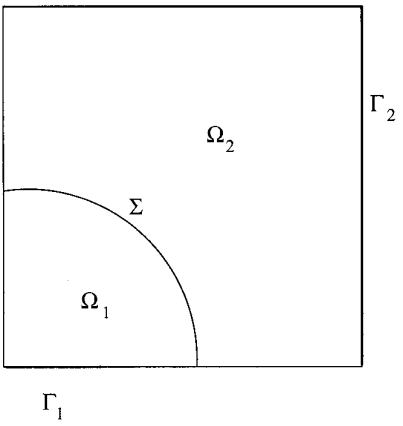

FIG. 8. Domain of solution.

$$u_o = -(x^3 + y^3) \quad \text{on } \Gamma_1 \cup \Sigma \tag{53}$$

and the solution in Ω_2 is subject to

$$u_o = x^3 + y^3 \quad \text{on } \Gamma_2 \cup \Sigma. \tag{54}$$

The inner solution is valid near the boundary and interior layers and it satisfies

$$\frac{d^2 u_i}{d\xi^2} - u_i = 0 \quad \forall \eta \in \Sigma \cup \Gamma_1 \cup \Gamma_2. \tag{55}$$

Equation (55) is subjected to boundary conditions (17), (18). The outer solution is plotted in Fig. 9a. After correction in the layer regions and an improvement step we get the solution (Fig. 9b). Our coarse mesh solution is based on five elements, each of order 5 in the x and y directions. The differences between our solution and a fully numerical solution are plotted in Figs. 9c, d.

8. CONCLUSIONS

The aim of this work was to present an efficient high-order method of some generality for the solution of multidimensional problems with boundary and interior layers. Our approach exploits the fact that the boundary layer can be approximately treated as a one-dimensional problem. In that way, the solution is straightforward and does not depend on the dimensionality of the problem. The solution away from the boundary layer is obtained by using a spectral element method. The number of degrees of freedom required to obtain the solution is small, because the outer solution does not have a boundary layer and, thus, the spectral convergence is retained. In order to deal with both boundary and interior layers, we used a penalty spectral element method for the numerical solution so that the outer solution and the improved solution are calculated on the same grid and there is no need to

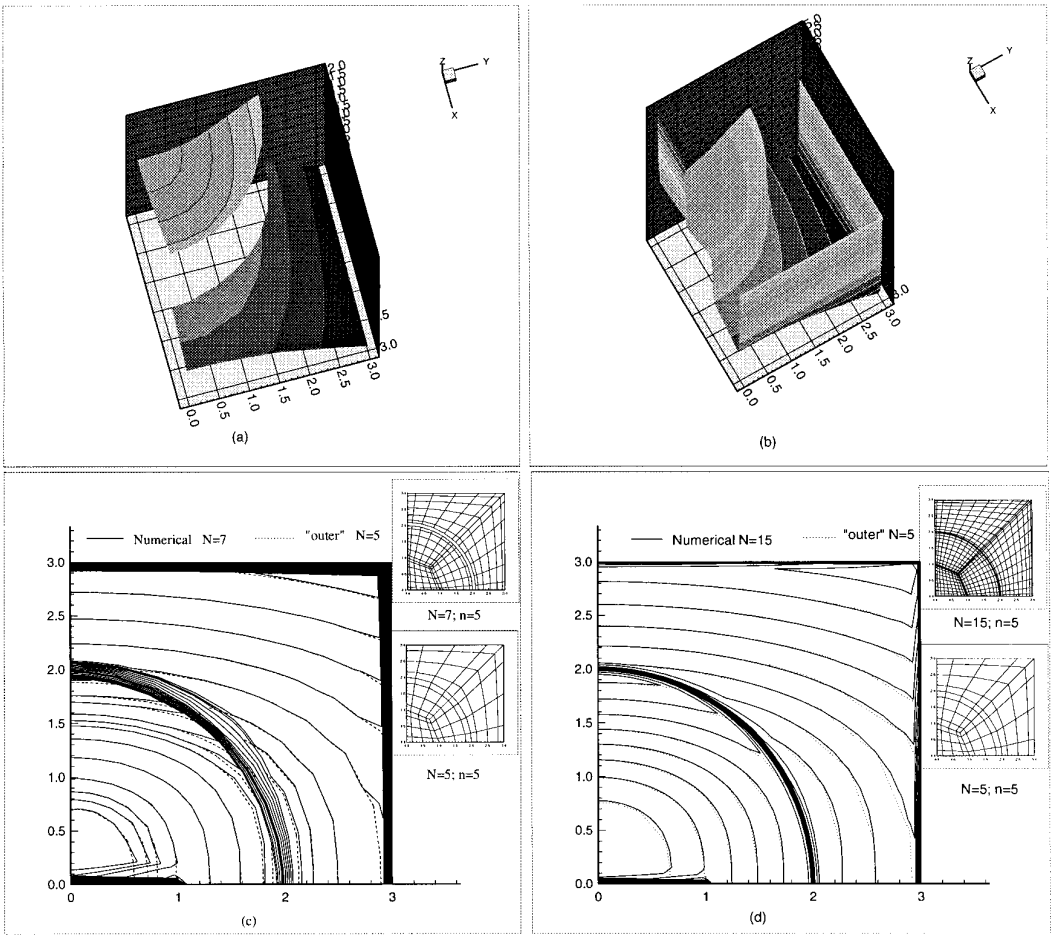

FIG. 9. Two-dimensional problem with interior and boundary layer ($\varepsilon = 1 \times 10^{-6}$): (a) Outer solution; (b) Improved solution; (c) Numerical solution, $N = 7$; $n = 5$; (d) Numerical solution, $N = 15$; $n = 5$.

change the structure of the coefficient matrices. We believe that the new method will be useful for a variety of problems involving interior and boundary layers, such as semiconductor device simulation problems [15, 16].

ACKNOWLEDGMENTS

This research was supported by *ONR/ARPA* under Contract *N*00014-92-*J*-1796.

REFERENCES

1. J. Kevorkian and J. D. Cole, *Perturbation Methods in Applied Mathematics,* Appl. Math. Sci., Vol. 34 (Springer-Verlag, New York, 1981).
2. P. A. Markowich, *The Stationary Semiconductor Device Equations* (Springer-Verlag, New York, 1984).

3. M. Van Dyke, *Perturbation Methods in Fluid Mechanics* (Academic Press, New York, 1964).
4. J. J. H. Miller (Ed.), *Boundary and Interior Layers: Computational and Asymptotic Methods: Proceedings of the BAIL I Conference, Trinity College, Dublin, 3–6 June, 1980* (Boole Press, Dublin, Ireland, 1980).
5. M. Israeli and M. Ungarish, Improvement of numerical solutions of boundary value problems by incorporation of asymptotic approximations, *Numer. Math.* **39,** (1982).
6. I. Babuska, O. C. Zienkiewicz, J. Gago, and E. R. Oliveria (Eds.), *Accuracy Estimates and Adaptive Refinements in Finite Element Computations* (Wiley, New York, 1986).
7. G. Strang and G. Fix, *An Analysis of the Finite Element Method* (Prentice Hall, Englewood Cliffs, NJ, 1973).
8. Y. Maday, C. Bernardi, and A. T. Patera, A new nonconforming approach to domain decomposition: The mortar element method, in *Nonlinear Partial Differential Equations and Their Applications, College de France Seminar,* edited by H. Brezis and J. L. Lions (Pitman, New York, 1989).
9. C. Mavriplis, *Nonconforming Discretizations and a Posteriori Error Estimators for Adaptive Spectral Elements Techniques, Ph.D. thesis,* M.I.T., 1989.
10. J. F. Flaherty and R. E. O'Malley Jr., The numerical solution of boundary value problems for stiff differential equations, *Math. Comput.* **31,** 66 (1977).
11. P. Bar-Yoseph and M. Israeli, An asymptotic finite element method for improvement of solutions of boundary layer problems. *Int. J. Numer. Methods Fluids* **6,** 21 (1986).
12. P. Bar-Yoseph, M. Israeli, and S. Weichendler, The asymptotic spectral element method, in *2nd Int. Conf. on Spectral and High Order Methods, June 22–26, 1989.*
13. R. B. Kellogg and A. Tsan, Analysis of some difference approximations for a singular perturbation problem without turning points, *Math. Comput.* **32,** 1025 (1977).
14. A. T. Patera, A spectral element method for fluid dynamics: Laminar flow in a channel expansion, *J. Comput. Phys.* **54,** 468 (1984).
15. I. Efrat and M. Israeli, A hybrid solution of the semiconductor device equations, in *Proceedings, Nasecode VII, 1991.*
16. U. Zrahia and S. A. Orszag, Mixed Legendre/Laguerre-spectral element algorithm for efficient solution of non linear problems with interior or boundary layers, in preparation.